# Heat and Mass Transfer in Partial Enclosures

K. Vafai* and S. Sarkar†
*Ohio State University, Columbus, Ohio*

**The present investigation is about the condensation and phase change processes in an enclosure partially filled with a porous insulation. The effect of variations in the porous insulation thickness on the moisture, relative humidity, temperature, and condensation rate fields is investigated. The problem is modeled as a transient, multiphase flow in a composite slab consisting of a porous portion followed by an air gap with impermeable, adiabatic horizontal boundaries and permeable vertical boundaries. The thickness of the porous insulation is varied between 60 and 100% of the overall thickness of the enclosure. For some typical conditions in a building insulation, it is found that the condensation rate and the resultant liquid accumulation do not increase significantly as the thickness of the insulation is decreased in the aforementioned range.**

## Nomenclature

$a$ = fraction of the enclosure filled with insulation
$\bar{c}$ = heat capacity at constant pressure, W · s/kg · K
$\bar{D}_1$ = vapor diffusivity coefficient, m²/s
$\bar{D}_{1,\text{eff}}$ = effective vapor diffusivity coefficient in the porous medium, m²/s
$\bar{D}_{1,\text{air}}$ = vapor diffusivity coefficient in air, m²/s
$Fo$ = Fourier number, $\bar{\alpha}_{0,\text{eff}}\bar{t}/\bar{L}^2$
$\Delta\bar{h}_{\text{vap}}$ = enthalpy of vaporization per unit mass, W · s/kg
$\bar{K}$ = thermal conductivity, W/m · K
$\bar{K}_{\text{eff}}$ = effective thermal conductivity, W/m · K
$\bar{L}$ = characteristic length of the insulation, m
$Le_1$ = Lewis number in the porous insulation, $\bar{\alpha}_{0,\text{eff}}/\bar{D}_{1,\text{eff}}$
$Le_2$ = modified Lewis number in the air gap, $\bar{\alpha}_{0,\text{eff}}/\bar{D}_{1,\text{air}}$
$\dot{m}$ = dimensionless rate of phase change (negative for condensation and positive for evaporation), $\bar{\dot{m}}/(\bar{\rho}_0\bar{c}_0\,\Delta\bar{T}\bar{\alpha}_{0,\text{eff}}/\bar{L}^2\,\Delta\bar{h}_{\text{vap}})$
$Pe$ = Peclet number, $\bar{V}_0\bar{L}/\bar{\alpha}_{0,\text{eff}}$
$\bar{R}_1$ = vapor gas constant, N · m/kg · K
$t$ = dimensionless time, $\bar{t}/(\bar{L}^2/\bar{\alpha}_{0,\text{eff}}) = Fo$
$T$ = dimensionless temperature, $\bar{T}/\Delta\bar{T}$
$x$ = dimensionless spatial coordinate, horizontal
$\bar{V}_0$ = infiltration velocity, m/s
$\bar{\alpha}_{0,\text{eff}}$ = effective reference thermal diffusivity, m²/s
$\Delta\bar{T}$ = reference temperature difference, K
$\epsilon$ = volume fraction
$\rho$ = dimensionless density
$\bar{\rho}_{1,s}$ = saturated vapor density, kg/m³
$\omega$ = relative humidity, $\bar{\rho}_1/\bar{\rho}_{1,s}$

*Subscripts*

$c$ = cold boundary
eff = effective properties
$h$ = hot boundary
$s$ = saturated vapor
$\beta$ = liquid phase
$\gamma$ = gas phase, which consists of air and water vapor
$\sigma$ = solid phase
0 = reference properties and variables
1 = vapor phase
2, air = air phase

*Superscripts*

$(\bar{\ })$ = dimensional quantities
$\gamma$ = intrinsic phase averages in the gaseous phase
$\langle\ \rangle$ = local volume average of a quantity

## Introduction

THE subject of partially filled enclosures has very recently received some attention.[1] The basic reason for this recent interest is the feasibility of obtaining the same thermal insulation for an enclosure partially filled with insulation as for an enclosure completely filled with insulation.

A typical fibrous insulation consists of a solid matrix in a gas phase consisting of a mixture of air, water vapor, and a very small amount of adsorbed liquid water. Condensation may occur in the interior of the insulation if the heat losses decrease the vapor temperature to its saturation value. This results in augmented heat transfer as a result of the liberated latent heat of evaporation. Condensation also leads to an increase in the apparent thermal conductivity of an insulation slab as the thermal conductivity of water is approximately 24 times that of air. Energy transfer in the fibrous insulation involves several different transport mechanisms. There is heat conduction in all the three phases. Vapor diffusion and convection occur in the gas phase due to density variations induced by temperature and vapor concentration gradients.[2-6,9] Infiltration occurs as a result of the pressure drop across the insulation walls, which has to be accounted properly.

In many applications, an enclosure of fibrous insulation separates the warm, humid air from a colder environment, as shown in Fig. 1a. However, in this work only a fraction of the enclosure consists of the fibrous insulation with the remaining empty space forming an air gap. The problem is modeled as a transient, multiphase flow in a porous slab with impermeable, adiabatic horizontal boundaries and permeable vertical boundaries. The insulation matrix is assumed to have a large aspect ratio, i.e., a large height-to-gap ratio, and a small modified Rayleigh number. Furthermore, it is assumed that the bulk velocity in the gas phase is due to infiltration and the liquid accumulation is small so that it exists in the pendular form. An investigation of the interaction between moisture, relative humidity, temperature, and the condensation rate fields for different insulation thicknesses is presented. The interface between the dry and wet zones is found directly from the solution of the transient governing equations. The present

Received Feb. 24, 1986; revision received June 20, 1986. Copyright © 1987 by K. Vafai. Published by the American Institute of Aeronautics and Astronautics, Inc., with permission.

*Associate Professor, Department of Mechanical Engineering.
†Presently Graduate Student, Department of Mechanical Engineering, Cornell University, Ithaca, NY.

investigation neglects natural convection in the air gap of the partial insulation enclosure, although heat transfer by infiltration and mass transfer are accounted for. Neglecting the natural convection in the air gap is not a good assumption if the air gap occupies a major fraction of the enclosure. Therefore, instead of varying the insulation thickness 0–100% of the overall thickness of the enclosure, the range of variation has been limited to 60–100% in the current work.

For some typical conditions in a building insulation, it was found that the condensation and the resultant liquid accumulation did not increase significantly as the thickness of the insulation was decreased by 40%. Thus, an enclosure partially filled with 60% or more of an insulation material seems to be as good, as far as the condensation problem is concerned, as an enclosure completely filled with an insulation material.

## Analysis

The problem is modeled as a slab partially filled with an insulation material as shown in Figs. 1b and 1c. The vertical boundaries are permeable to matter as well as heat. When the temperature and vapor density gradients are moderate, the liquid accumulation by phase change is small[6] and therefore the condensate is usually present in a discontinuous and pendular state.[7] Hence, vapor transfer, and not liquid transfer, is the dominant mode of moisture transport. Furthermore, moderate temperature gradients and the large aspect ratio of a typical fibrous insulation greatly reduce the free-convection heat-transfer process.

However, the bulk convection due to air infiltration is usually very important and must be considered. Therefore, in this work the enclosure is assumed to have a large aspect ratio and a small modified Rayleigh number. It is also assumed that the bulk velocity in the gas phase is due to infiltration and the porous insulation is homogeneous and isotropic. The governing equations for the porous section that are valid in the range of $0 < x < a$ are then obtained as

$$\frac{\partial \epsilon_\beta}{\partial t} + \frac{\langle \dot{m} \rangle}{S_1 S_2} = 0 \tag{1}$$

$$\frac{\partial}{\partial t}(\epsilon_\gamma \langle \rho_\gamma \rangle^\gamma) + Pe \frac{\partial \langle \rho_\gamma \rangle^\gamma}{\partial x} - \frac{\langle \dot{m} \rangle}{S_4 S_2} = 0 \tag{2}$$

$$\frac{\partial}{\partial t}(\epsilon_\gamma \langle \rho_1 \rangle^\gamma) + Pe \frac{\partial}{\partial x} \langle \rho_1 \rangle^\gamma - \frac{\langle \dot{m} \rangle}{S_4 S_2 S_5} = \frac{1}{Le_1} \frac{\partial}{\partial x}\left[ \langle \rho_\gamma \rangle^\gamma \frac{\partial}{\partial x}\left( \frac{\langle \rho_1 \rangle^\gamma}{\langle \rho_\gamma \rangle^\gamma} \right) \right] \tag{3}$$

$$\frac{\partial \langle T \rangle}{\partial t} + \frac{S_3 S_4 S_6 Pe}{S_7} \langle \rho_\gamma \rangle^\gamma \frac{\partial \langle T \rangle}{\partial x} + \frac{S_6}{S_7} \langle \dot{m} \rangle = \frac{S_6}{S_7} \frac{\partial}{\partial x}\left[ S_7 \frac{\partial \langle T \rangle}{\partial x} \right] \tag{4}$$

$$\epsilon_\sigma + \epsilon_\beta + \epsilon_\gamma = 1 \tag{5}$$

where

$$S_1 = \frac{\bar{\rho}_\beta}{\bar{\rho}_0}, \quad S_2 = \frac{\Delta \bar{h}_{vap}}{\bar{c}_0 \, \Delta \bar{T}}, \quad S_3 = \frac{\langle \bar{c}_\gamma \rangle^\gamma}{\bar{c}_0} \tag{6}$$

$$S_4 = \frac{\bar{\rho}_{\gamma,0}}{\bar{\rho}_0}, \quad S_5 = \frac{\bar{\rho}_{1,0}}{\bar{\rho}_{\gamma,0}}, \quad S_6 = \frac{\bar{\alpha}_{eff}}{\bar{\alpha}_{0,eff}} \tag{7}$$

$$S_7 = \frac{\bar{K}_{eff}}{\bar{K}_{0,eff}}, \quad Pe = \frac{\bar{V}_0 \bar{L}}{\bar{\alpha}_{0,eff}}, \quad Le_1 = \frac{\bar{\alpha}_{0,eff}}{\bar{D}_{1,eff}} \tag{8}$$

The above equations are obtained after considerable algebraic manipulations on the work of Whitaker on drying.[2] The above equations neglect any boundary and inertia effects. This is a reasonable assumption for the present problem based on the analysis of Vafai and Tien.[8,10] Therefore the above equations are based on the Darcy formulation.[11,13] In developing the governing equations, it is assumed that the effective vapor transport coefficient $\bar{D}_{1,eff}$ is a constant. However, without any available experimental data, the moisture transport coefficient is not a known quantity. Therefore, experimental investigations are needed in this area. The value of $\bar{D}_{1,eff}$ used in this analysis was $10^{-5}$ m$^2$/s. This value is based on the fact that the moisture transport coefficient is approximately dominated by the gas-phase diffusion for very small values of the liquid content.

In these equations, $\langle \rho_1 \rangle^\gamma$ and $\langle \rho_\gamma \rangle^\gamma$ are the intrinsic phase averages for $\rho_1$ and $\rho_\gamma$ in the gaseous phase and the bracketed variables refer to the local volume average of that variable. Equation (1) provides the history of the condensate in the porous section, Eqs. (2) and (3) the space and time variations of the gaseous density and the condensation rate, respectively, Eq. (4) the transient behavior of the temperature distribution inside of the porous section, and Eq. (5) a volumetric constraint at any point in space and at any time. The quantities with subscript "0" refer to the reference properties and variables and the variables with bar on top to dimensional quantities. The reference properties refer to typical properties of a fibrous insulation material. It should be noted that the reference properties are calculated when there is no phase change in the insulation material. However, as the insulation material experiences a phase change, the properties will change (these variable properties are accounted for in the analysis). For this reason, the original properties are named reference properties.

The Peclet number $Pe$ characterizes the relative importance of the convective and diffusive heat-transfer process. The Lewis

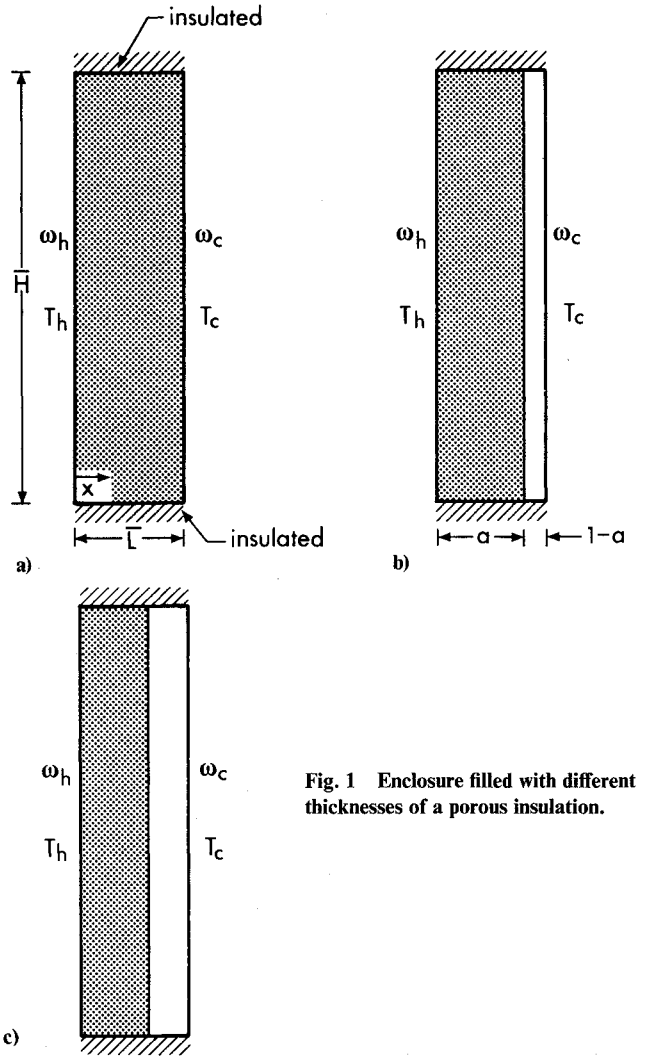


**Fig. 1 Enclosure filled with different thicknesses of a porous insulation.**

number $Le$ characterizes the relative importance of the heat- and mass-transport mechanisms. Both the Peclet and Lewis numbers are independent of space and time. Among the controlling parameters, $S_3$, $S_6$, and $S_7$ vary with transient and spatial variations of the thermophysical properties. On the other hand, $S_1$, $S_2$, $S_4$, and $S_5$ are constants that are fixed once the reference properties are chosen. At any location in the porous slab where it is dry, the condensation rate $\langle \dot{m} \rangle$ is identically zero. On the other hand, at any point in the slab where it is wet, the vapor density equates itself to the saturated vapor density, which is given by

$$\rho_{1,s} = \frac{1}{S_9 \langle T \rangle} \exp\left\{\frac{S_8}{\langle T \rangle} + \frac{S_8}{T_0}\right\} \tag{9}$$

where

$$S_8 = \frac{\Delta \bar{h}_{\text{vap}}}{\bar{R}_1 \Delta \bar{T}}, \qquad S_9 = \frac{\Delta \bar{T}}{\bar{T}_0} \tag{10}$$

For the air space, $a < x < 1$, the governing equations are obtained as

$$\frac{\partial \rho_\gamma}{\partial t} + Pe \frac{\partial \rho_\gamma}{\partial x} = 0 \tag{11}$$

$$\frac{\partial \rho_1}{\partial t} + Pe \frac{\partial \rho_1}{\partial x} = \frac{1}{Le_2} \frac{\partial}{\partial x}\left[\rho_\gamma \frac{\partial}{\partial x}\left(\frac{\rho_1}{\rho_\gamma}\right)\right] \tag{12}$$

$$\frac{\partial T}{\partial t} + Pe \frac{\partial T}{\partial x} = S_{10} \frac{\partial^2 T}{\partial x^2} \tag{13}$$

where

$$Le_2 = \frac{\bar{\alpha}_{0,\text{eff}}}{\bar{D}_{1,\text{air}}}, \qquad S_{10} = \frac{\bar{\alpha}_{\text{air}}}{\bar{\alpha}_{0,\text{eff}}} \tag{14}$$

In the above, Eqs. (11) and (12) provide the transient distributions of the gaseous and vapor densities, and Eq. (13) gives the temperature distribution inside the air gap. Details about the interface boundary conditions are given in the next section.

To investigate the effect of partial insulation on the condensation and temperature distributions, Eqs. (1–5), (9), and (11–13), which are nonlinear and coupled, are solved subject to a typical set of boundary and initial conditions.

## The Numerical Scheme

Since the governing equations for the partially filled slab are nonlinear and coupled, a numerical scheme was devised for solving the governing equations.

The numerical scheme was based on the finite-difference form of Eqs. (1–5) and (11–13). The space derivatives were approximated by a central-differences form except for the convective terms, which were approximated by using an upwind differencing scheme. The accuracy of the numerical solution was tested by decreasing the spatial and time increments and comparing the corresponding values of the pertinent variables in both cases. In solving Eqs. (1–5) inside the porous slab, two different approaches were pursued. Based on the experimental results of Langlais et al.,[6] values of $\epsilon_\beta < 10^{-6}$ were considered to be part of the adsorbed water. Therefore, when $\epsilon_\beta$ was less than $10^{-6}$, the condensation rate was set equal to zero at that location in the slab. This way, for $\epsilon_\beta < 10^{-6}$, Eq. (9) was not used in the numerical solution.

The interface between this porous slab and the air space requires special consideration. This is due to the sharp change of properties across the interface. Let nodes $(m-2)$ and $(m-1)$ denote the region inside the porous slab next to the interface and the nodes $m$ and $(m+1)$ denote the region inside the air gap next to the interface. Therefore, the control volumes corresponding to the nodes $(m-1)$ and $m$ have a common boundary exactly at the interface. In the numerical scheme, the governing equations corresponding to the porous slab are applied up to and including node $(m-2)$, and for node $(m+1)$ and beyond the governing equations for the air gap are applied. However, nodes $(m-1)$ and $m$ require special handling. This is done by allowing the thermal conductivity and the diffusivity coefficient to vary across the control volumes corresponding to nodes $(m-1)$ and $m$. Following Patankar's[14] approach, we define a new set of interface properties for the thermal conductivity and the diffusivity coefficient. For the present case, these are obtained as

$$\bar{K}_i = \frac{2\bar{K}_{\text{eff}}\bar{K}_{\text{air}}}{\bar{K}_{\text{eff}} + \bar{K}_{\text{air}}} \tag{15}$$

$$\bar{D}_i = \frac{2\bar{D}_{\text{i,eff}}\bar{D}_{1,\text{air}}}{\bar{D}_{1,\text{eff}} + \bar{D}_{1,\text{air}}} \tag{16}$$

Now the thermal conductivity and diffusivity coefficients $\bar{K}$ and $\bar{D}_1$ are allowed to vary from $\bar{K}_{\text{eff}}$ and $\bar{D}_{1,\text{eff}}$ to $\bar{K}_i$ and $\bar{D}_i$ across the control volume corresponding to node $(m-1)$ inside the porous slab. Likewise, these coefficients, $\bar{K}$ and $\bar{D}_1$, are allowed to vary from $\bar{K}_i$ and $\bar{D}_i$ to $\bar{K}_{\text{air}}$ and $\bar{D}_{1,\text{air}}$ across the control volume corresponding to node $m$ inside the air gap. To account for these variations, Eq. (3), which corresponds to the porous side, and Eqs. (12) and (13), which correspond to the air gap, need to be modified. Therefore, for node $(m-1)$ Eqs. (1), (2), (4), and (5) are still utilized. However, instead of Eq. (3), the following equation was used:

$$\frac{\partial}{\partial t}(\epsilon_\gamma \langle \rho_1 \rangle^\gamma) + Pe \frac{\partial \langle \rho_1 \rangle^\gamma}{\partial x} - \frac{\langle \dot{m} \rangle}{S_2 S_4 S_5} = \frac{\partial}{\partial x}\left[\frac{1}{Le_1^*}\langle \rho_\gamma \rangle^\gamma \frac{\partial}{\partial x}\left(\frac{\langle \rho_1 \rangle^\gamma}{\langle \rho_\gamma \rangle^\gamma}\right)\right] \tag{17}$$

where $Le_1^* = \bar{\alpha}_{0,\text{eff}}/\bar{D}$ varies across the control volume for node $(m-1)$.

For the air gap for node $m$, Eq. (11) is still used; however, instead of Eqs. (12) and (13), the following were used:

$$\frac{\partial \rho_1}{\partial t} + Pe \frac{\partial \rho_1}{\partial x} = \frac{\partial}{\partial x}\left[\frac{1}{Le_2^*}\rho_\gamma \frac{\partial}{\partial x}\left(\frac{\rho_1}{\rho_\gamma}\right)\right] \tag{18}$$

$$\frac{\partial T}{\partial t} + Pe \frac{\partial T}{\partial x} = \frac{S_{10}}{S_{11}} \frac{\partial}{\partial x}\left[S_{11}^* \frac{\partial T}{\partial x}\right] \tag{19}$$

$$Le_2^* = \frac{\bar{\alpha}_{0,\text{eff}}}{\bar{D}}, \qquad S_{11}^* = \frac{\bar{K}}{\bar{K}_{0,\text{eff}}} \tag{20}$$

where $Le_2^*$ and $S_{11}^*$ vary across the control volume for node $m$. Thus, in order to account for the interface between the air gap and insulation, the values of the thermal diffusivity and vapor diffusivity have been appropriately varied across the interface.

## Results and Discussion

To investigate the effect of variations of the insulation thickness on the condensation process the insulation thickness was varied at 60–100% of the enclosure thickness. Specifically, three different insulation thicknesses were analyzed: 60, 80, and 100% of the enclosure thickness.

Initially, it was assumed that there was no water condensate inside the insulation slab. However, the solution scheme allowed for the presence of some initial adsorbed water inside the slab. Although the nonhomogeneity near the insulation boundaries could be considered by letting the fiber porosity be a function of position, in the present analysis the fiber porosity was considered to be a constant. In analyzing the condensation process, the physical data, which correspond to some typical conditions in a building insulation, shown in Table 1 were used in the numerical calculations. It should be noted that $\Delta \bar{T}$ is not

related to $\bar{T}_h$ and $\bar{T}_c$—it represents only a characteristic temperature difference.

The boundary conditions on the temperature and the relative humidity were specified for a hot and humid environment on one side and a colder environment on the other. These boundary conditions are specified as

$$T(x=0,t)=15.65$$
$$T(x=1,t)=15.0$$
$$T(x,t=0)=15.0 \qquad (21)$$

and

$$\omega(x=0,t)=\omega_h$$
$$\omega(x=1,t)=\omega_c=1$$
$$\omega(x,t=0)=1 \qquad (22)$$

For all of the figures presented in this section, an $\omega_h$ of 0.6 was used in the numerical computations. The transient analysis of the process is very important because a typical insulation slab is exposed to a natural cyclic behavior on a day-to-day basis. In what follows, the interaction between the liquid fraction, condensation rate, relative humidity, and temperature fields for three different insulation thicknesses is presented.

First, the case where the entire enclosure is filled with the porous insulation is considered. The time history of the liquid fraction at three different spatial locations, $x_1=0.2$, $x_2=0.6$, and $x_3=0.8$, is presented in Fig. 2a. The spatial distribution of the liquid content at three different times, $\bar{t}_1=250$ s, $\bar{t}_2=500$ s, and $\bar{t}_3=2000$ s, is shown in Fig. 2b. The time history and spatial distribution of the condensate rate, for the same spatial and time locations as in Fig. 2, are presented in Figs. 3a and 3b, respectively. The relative humidity, defined as $\omega=\bar{\rho}_l/\bar{\rho}_{l,s}$, as a function of position inside of the slab is presented in Fig. 4a for the three different times used in Figs. 2 and 3. The temperature distribution at $t_1$, $t_2$, and $t_3$ is presented in Fig. 4b. There is condensation followed by subsequent drying in the porous slab as shown in Fig. 3a. The initial condensation occurs because the humid air from the exterior penetrates rapidly into the

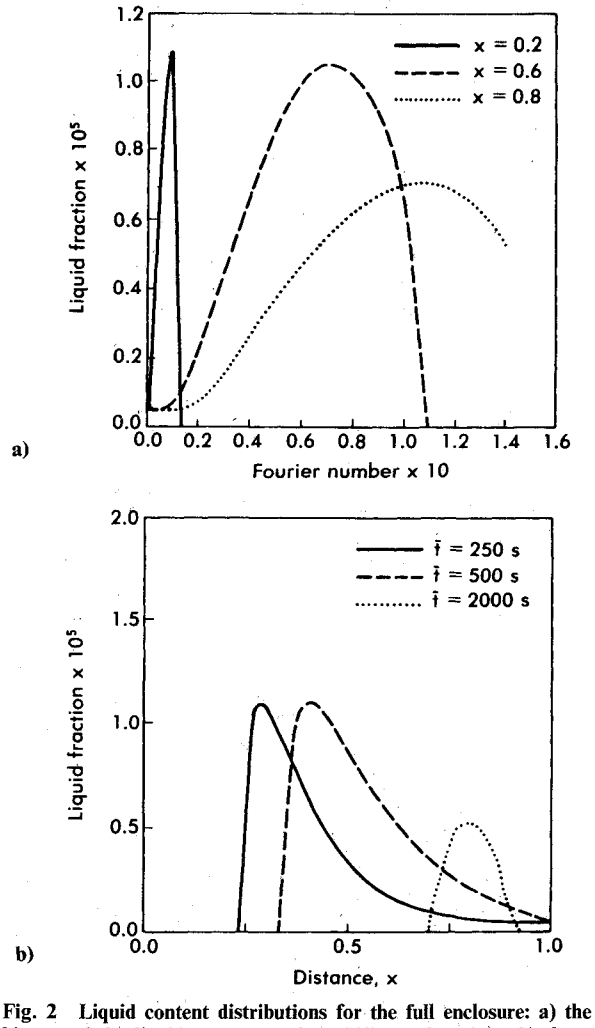


**Fig. 2 Liquid content distributions for the full enclosure: a) the time history of the liquid content at three different locations; b) the spatial distribution of the liquid fraction at three different times.**

**Table 1 Data used in analysis of condensation process**

| | |
|---|---|
| Physical properties | |
| $\epsilon_\sigma=0.03$ | $\bar{K}_{0,\text{eff}}=0.026$ W/m · K |
| $\bar{D}_{l,\text{eff}}=10^{-5}$ m²/s | $\bar{T}_h=313$ K |
| $\bar{\rho}_0=31$ kg/m³ | $\bar{T}_c=300$ K |
| $\alpha_{0,\text{eff}}=9.9\times10^{-7}$ m²/s | $\Delta\bar{T}=20$ K |
| $\bar{c}_0=842$ J/kg · K | $\bar{v}_0=1.66\times10^{-5}$ m/s |
| Air properties | |
| $\bar{\rho}_{\text{air}}=1.16$ kg/m³ | $\bar{D}_{\text{air}}=3\times10^{-5}$ m²/s |
| $\bar{c}_{\text{air}}=1000$ J/kg · K | $\bar{L}=0.12$ m |
| $\bar{K}_{\text{air}}=0.026$ W/m · K | |

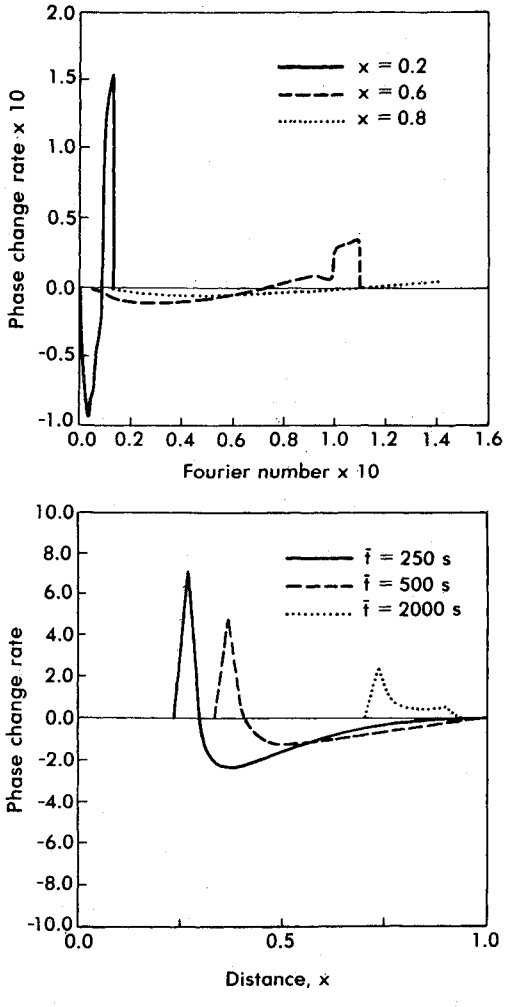


**Fig. 3 Condensation rate distribution for the full enclosure: a) the time history distributions; b) the spatial distributions.**

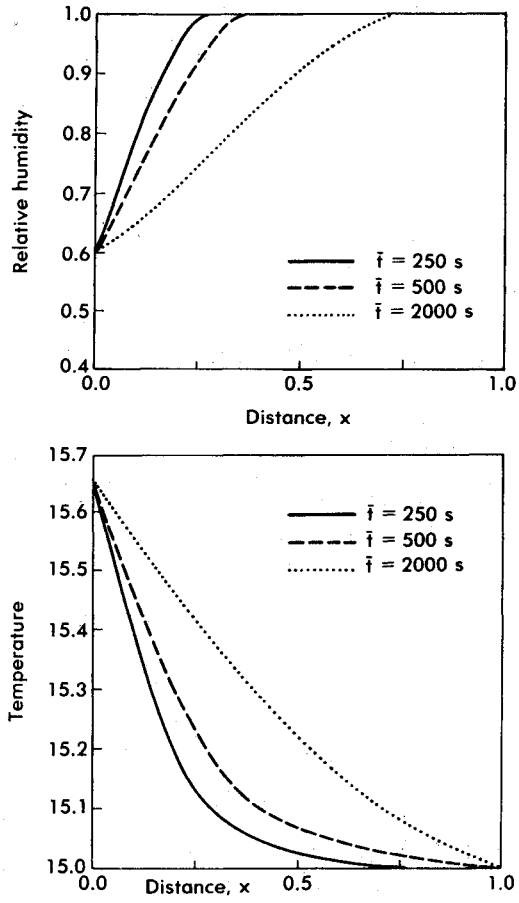


Fig. 4 Spatial distributions at three different times for a) relative humidity and b) temperature (for a full enclosure).

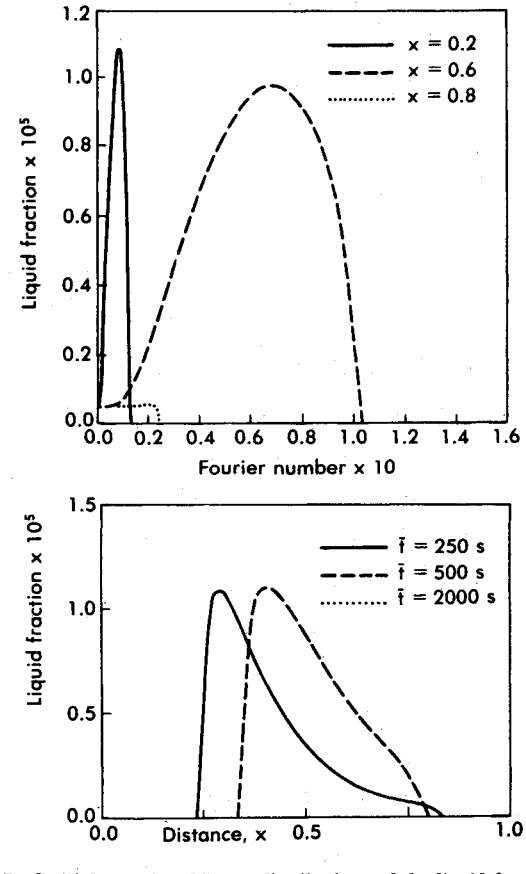


Fig. 5 Spatial and time history distributions of the liquid fraction for the 80% enclosure for the same spatial and time locations used in Fig. 2.

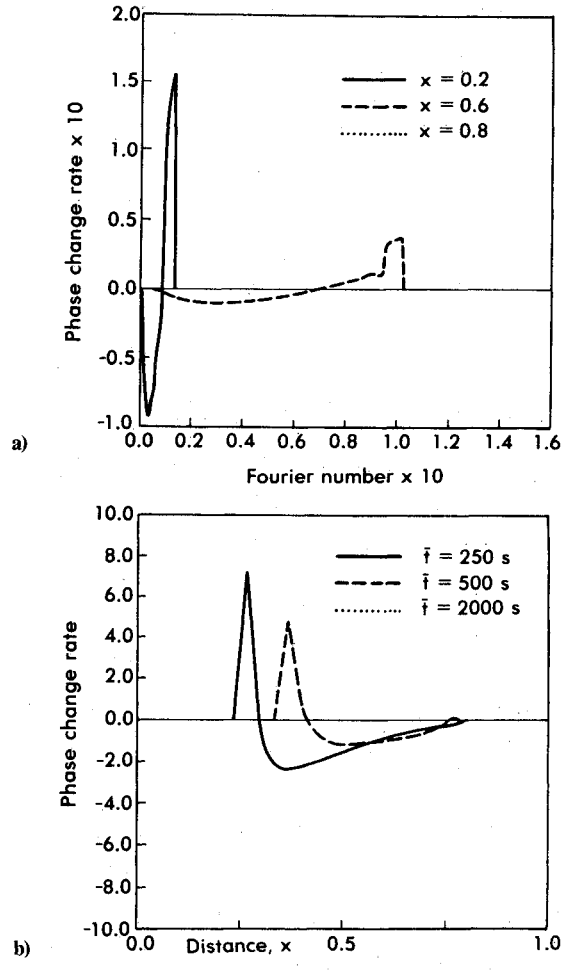


Fig. 6 Spatial and time history distributions of the condensation rate for the 80% partial enclosure for the same spatial and time locations used in Fig. 3.

cooler interior of the slab. However, since the temperature increases with time in the interior, as depicted by Fig. 4b, the accumulated liquid evaporates at later times. This evaporation process then results in an increase in the relative humidity as shown in Fig. 4a. Furthermore, it can be seen that in all of the figures that at time $\bar{t}_3$ the overall phase change rate and the liquid fraction have either become significantly reduced or have approached zero.

In a recent study of fibrous insulation,[15] it was shown that the condensation, and the resulting augmentation of heat transfer, is a serious problem only for large Peclet numbers (certainly for Peclet numbers above 1). For this reason, the Peclet number used in this investigation was chosen to be 2. This Peclet number corresponds to an infiltration velocity of $1.66 \times 10^{-5}$ m/s. This type of velocity can be easily induced by air infiltration through cracks and pinholes in the insulation boundaries. The corresponding spatial and transient field distributions, for the case when the insulation thickness is 80% of the enclosure thickness, are presented in Figs. 5–7. Finally the field distributions for the case where the insulation thickness is 60% of the full enclosure are presented in Figs. 8–10.

The abrupt changes in some of the field variables, shown in some of the figures, are believed to be the result of the complex interaction of the temperature and moisture fields. This complex interaction, along with the application of a step change in the boundary conditions, does not allow for a smooth evolution of field variables. The grid steps were doubled to check the effect of the grid sizes on these abrupt changes. It was found that, in general, the curves became smoother; however, the very abrupt changes and the qualitative behavior of the curves were not affected by the increase in the grid sizes. This was found to be true for all of the figures presented in this paper.

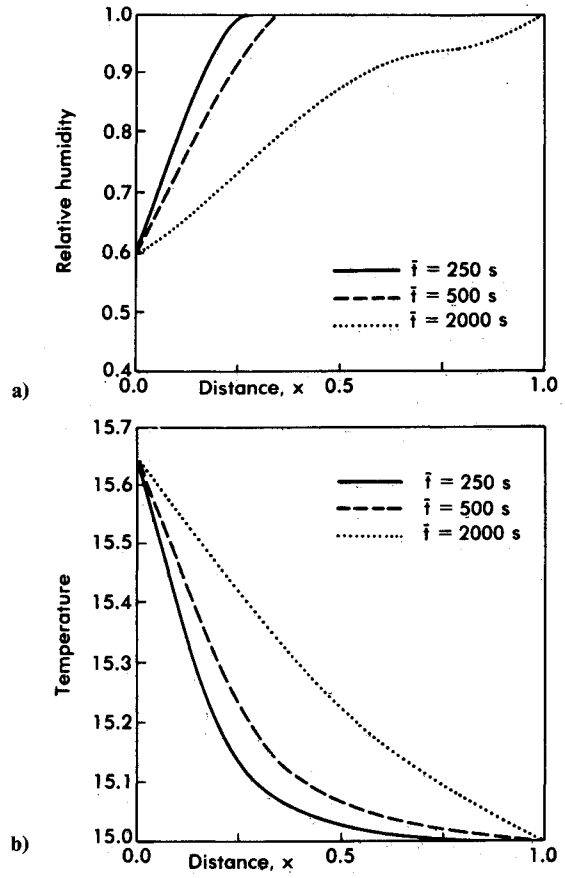


Fig. 7 The spatial distributions for a) relative humidity and b) temperature (for the 80% partial enclosure).

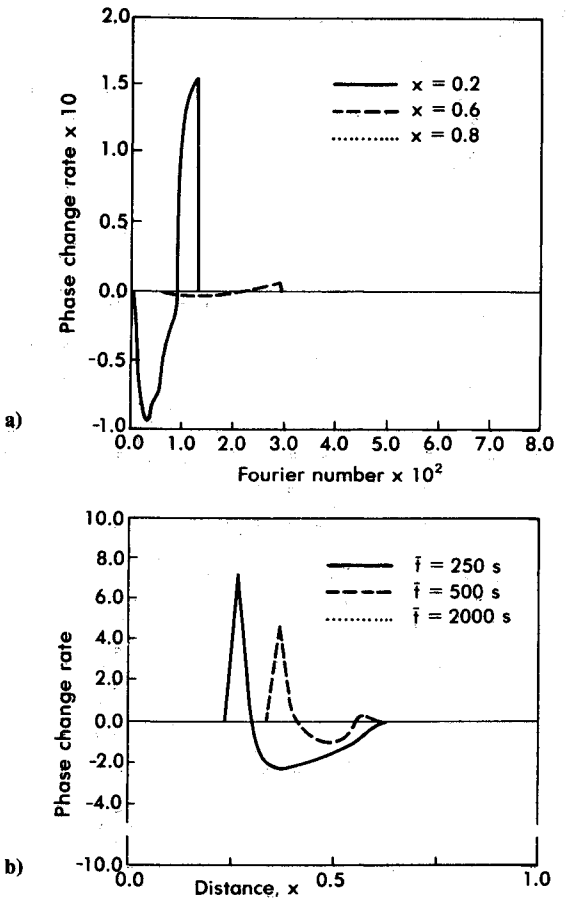


Fig. 9 Spatial and time history distributions of the condensation rate for the 60% partial enclosure.

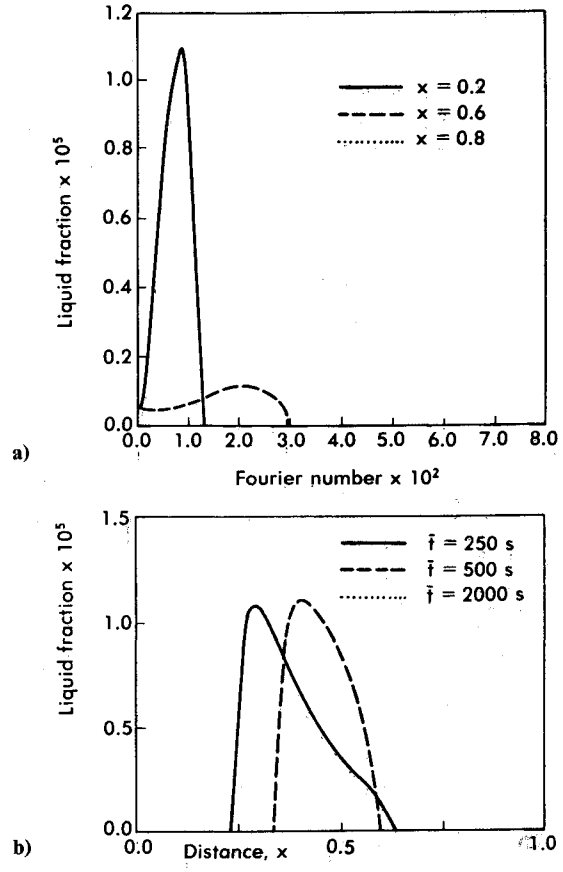


Fig. 8 Spatial and time history distributions of the liquid fraction for the 60% partial enclosure.

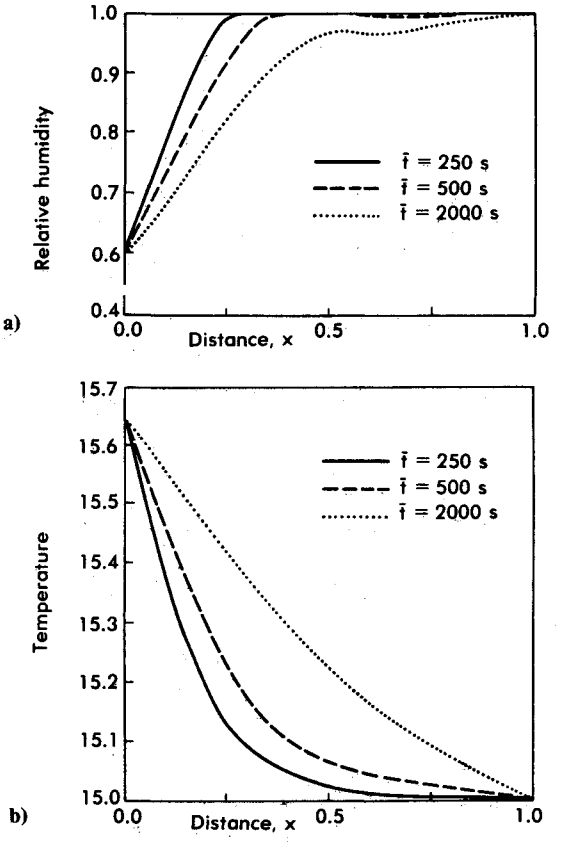


Fig. 10 Spatial distributions for the 60% partial enclosure: a) relative humidity; b) temperature.

As it can be seen, there is no major increase in the condensation rate or the liquid fraction for the partial enclosure and, in fact, these quantities were somewhat decreased at some time and spatial locations. The relative humidity does not experience any changes for the initial time; however, it experiences some changes for the later times. As for the temperature distribution, there is hardly any change at all for the full, 80%, and 60% partial enclosures at any time. In conclusion, an enclosure with insulation covering 60% or more of its length seems to be as good as a full enclosure as far as the condensation problem is concerned. The implications of these results are obvious, but very important. This is because of the savings in both the labor and material involved in installing these insulations for different applications.

## References

[1]Tong, T. W. and Subramanian, E., "Natural Convection in Rectangular Enclosures Partially Filled with a Porous Medium," *International Journal of Heat and Fluid Flow*, to be published.

[2]Whitaker, S., "Simultaneous Heat, Mass and Momentum Transfer in Porous Media," *A Theory of Drying, Advances in Heat Transfer*, Vol. 13, Academic Press, New York, 1977.

[3]Whitaker, S., "Advances in Theory of Fluid Motion in Porous Media," *Industrial and Engineering Chemistry*, Vol. 61, Dec. 1969, pp. 14–28.

[4]Luikov, A. V., *Heat and Mass Transfer in Capillary-Porous Bodies*, Pergamon, Oxford, England, 1966.

[5]Eckert, E. R. G. and Faghri, M., "Moisture Migration in an Unsaturated Porous Medium," *International Journal of Heat and Mass Transfer*, Vol. 23, Dec. 1980, pp. 1613–1623.

[6]Langlais, C., Hyrien, M., and Karlsfeld, S., "Moisture Migration in Fibrous Insulating Material Under the Influence of a Thermal Gradient, Moisture Migration in Buildings," ASTM STP 779, 1982, pp. 191–206.

[7]Ceaglske, N. M. and Hougen, O. A., "Drying Granular Solids," *Industrial and Engineering Chemistry*, Vol. 29, July 1937, pp. 805–813.

[8]Vafai, K. and Tien, C. L., "Boundary and Inertia Effects on Flow and Heat Transfer in Porous Media," *International Journal of Heat and Mass Transfer*, Vol. 24, Feb. 1981, pp. 195–203.

[9]Eckert, E. R. G. and Pfender, E., "Heat and Mass Transfer in Porous Media," *Proceedings Sixth International Heat Transfer Conference*, Vol. 6, 1978, pp. 1–12.

[10]Vafai, K. and Tien, C. L., "Boundary and Inertia Effects on Flow and Heat Transfer in Porous Media," *International Journal of Heat and Mass Transfer*, Vol. 25, Aug. 1982, pp. 1183–1190.

[11]Cheng, P., "Heat Transfer in Geothermal Systems," *Advances in Heat Transfer*, Vol. 14, 1978, pp. 1–105.

[12]Cheng, P. and Minkowycz, W. J., "Free Convection About a Vertical Flat Plate Embedded in a Porous Medium with Application to Heat Transfer from a Dike," *Journal of Geophysics Research*, Vol. 82, May 1977, pp. 2040–2044.

[13]Scheidegger, A. E., *The Physics of Flow through Porous Media*, University of Toronto Press, Toronto, 1974, pp. 73–97.

[14]Patankar, S. V., *Numerical Heat Transfer and Fluid Flow*, McGraw-Hill, New York, 1980, pp. 41–74.

[15]Vafai, K. and Sarkar, S., "Condensation Effects in a Fibrous Insulation Slab," *Journal of Heat Transfer*, Vol. 108, Aug. 1986, pp. 667–675.

*From the AIAA Progress in Astronautics and Aeronautics Series...*

**ENTRY VEHICLE HEATING AND THERMAL PROTECTION SYSTEMS: SPACE SHUTTLE, SOLAR STARPROBE, JUPITER GALILEO PROBE—v. 85**

**SPACECRAFT THERMAL CONTROL, DESIGN, AND OPERATION—v. 86**

*Edited by Paul E. Bauer, McDonnell Douglas Astronautics Company and Howard E. Collicott, The Boeing Company*

The thermal management of a spacecraft or high-speed atmospheric entry vehicle—including communications satellites, planetary probes, high-speed aircraft, etc.—within the tight limits of volume and weight allowed in such vehicles, calls for advanced knowledge of heat transfer under unusual conditions and for clever design solutions from a thermal standpoint. These requirements drive the development engineer ever more deeply into areas of physical science not ordinarily considered a part of conventional heat-transfer engineering. This emphasis on physical science has given rise to the name, thermophysics, to describe this engineering field. Included in the two volumes are such topics as thermal radiation from various kinds of surfaces, conduction of heat in complex materials, heating due to high-speed compressible boundary layers, the detailed behavior of solid contact interfaces from a heat-transfer standpoint, and many other unconventional topics. These volumes are recommended not only to the practicing heat-transfer engineer but to the physical scientist who might be concerned with the basic properties of gases and materials.

*Volume 85—Published in 1983, 556 pp., 6 × 9, illus., $35.00 Mem., $55.00 List*
*Volume 86—Published in 1983, 345 pp., 6 × 9, illus., $35.00 Mem., $55.00 List*

TO ORDER WRITE: Publications Order Dept., AIAA, 1633 Broadway, New York, N.Y. 10019